Applied Catalysis B: Environmental 160–161 (2014) 217–226

Contents lists available at ScienceDirect

Applied Catalysis B: Environmental

journal homepage: www.elsevier.com/locate/apcatb

A novel and green method to synthesize CdSe quantum dots-modified TiO_2 and its enhanced visible light photocatalytic activity

Peng Wang, Danzhen Li*, Jing Chen, Xiaoyun Zhang, Jiangjun Xian, Xue Yang, Xiuzhen Zheng, Xiaofang Li, Yu Shao

Research Institute of Photocatalysis, State Key Laboratory of Photocatalysis on Energy and Environment, Fuzhou University, No. 523 GongYe Road, Fuzhou 350002, PR China

ARTICLE INFO

Article history:
Received 21 February 2014
Received in revised form 15 May 2014
Accepted 18 May 2014
Available online 27 May 2014

Keywords:
CdSe QDs-modified TiO_2
Photocatalysis
Quantum size effect
Active species
Visible light irradiation

ABSTRACT

In this paper, a facile and green method was employed to synthesize CdSe quantum dots (QDs)-modified TiO_2. It exhibited much higher photocatalytic activities than both TiO_2 and bulk CdSe-modified TiO_2 on degrading malachite green (MG) aqueous solution under visible light irradiation. The vital role that quantum size effect of CdSe QDs plays in enhancing photocatalytic properties of CdSe QDs-modified TiO_2 is discussed in detail for the first time. Due to the more negative conduction band potentials of CdSe QDs than that of bulk CdSe, the electron transfer rate from CdSe QDs to TiO_2 is much faster than that from bulk CdSe to TiO_2, which would be beneficial for an efficient charge carrier's separation. As a result, more quantities of active species ($O_2\bullet^-$, H_2O_2, $\bullet OH$) are generated during the photocataltytic reaction in CdSe QDs-modified TiO_2 system. This work could not only provide a facile and green strategy to fabricate semiconductor QDs-modified TiO_2 photocatalyst but also contribute to a deeper understanding of the specific role of semiconductor QDs during the photocatalytic reaction process.

1. Introduction

Titanium dioxide (TiO_2), as one of the most important photocatalysts, has attracted most widespread attention due to its chemical stability, nontoxicity and high photocatalytic activity under UV light irradiation [1,2]. However, the practical applications of the TiO_2 photocatalyst are limited by the ineffective utilization of visible light and low quantum efficiency [3,4]. Coupling TiO_2 with a narrow band gap semiconductor is an effective approach to overcome these drawbacks. For example, $LaVO_4/TiO_2$, $BiVO_4/TiO_2$, Ag_3VO_4/TiO_2, Bi_2WO_6/TiO_2, WO_3/TiO_2 have already been reported to exhibit excellent visible light photocatalytic activity [5–9]. Developing novel materials to couple with TiO_2 to broaden the responsive spectra region of TiO_2 and increase the quantum efficiency is still one of the research hotspot in the photocatalytic field.

As novel nanomaterials, semiconductor QDs often refer to nanocrystals with their particle sizes less than twice the Bohr radius of excitons in the bulk materials [10]. Semiconductor QDs have many unique properties such as quantum size effect [11] and multiple exciton generation effect [12] comparing to their bulk counterparts. Among the semiconductor QDs, CdSe QDs has attracted great attention in the past decades. To our knowledge, CdSe is an important II–VI group semiconductor with a direct energy band gap of 1.75 eV for bulk phase [13]. Particularly, CdSe has a higher conduction band edge than that of TiO_2 [14], which is beneficial for the injection of excited electrons from CdSe to TiO_2. Recently, CdSe sensitized TiO_2 has been widely investigated for photocatalytic water splitting for H_2 generation [15,16] and photoreduction of CO_2 [17]. However, relatively fewer reports have been focused on the utilization of CdSe sensitized TiO_2 for photocatalytic oxidization toward organic pollutants [18–23]. As a unique property of semiconductor QDs, quantum size effect has already been reported to have a great influence on the photocatalytic activity of QDs-based photocatalyst [24–29]. Yu et al. [30] reported that the quantum-sized CdSe nanoparticles enhanced the photocatalytic activity of the $CdSe/TiO_2$ coupled system toward degradation of 4-CP. However, the specific role that quantum size effect of CdSe QDs plays in $CdSe–TiO_2$ nanocomposite during the photocatalytic reaction has not been studied systematically. So it is of great value to investigate in detail the role of quantum size effect of CdSe QDs in improving activities of CdSe QDs-modified TiO_2.

Recently, linker-assisted hybridization method has become a common approach to immobilize CdSe QDs on the TiO_2 surface, which can be generally classified into two routes. One route is to functionalize oil soluble CdSe QDs with mercaptan acid by a ligand

* Corresponding author. Tel.: +86 591 83779256; fax: +86 591 83779256.
E-mail addresses: dzli@fzu.edu.cn, danzli@126.com (D. Li).

http://dx.doi.org/10.1016/j.apcatb.2014.05.032
0926-3373/

exchange process to get water soluble CdSe QDs solution, followed by immersing TiO_2 films to obtain the CdSe QDs decorated TiO_2 [31–33]. The other route is to functionalize TiO_2 films with mercaptan acid and then put it into as-prepared oil soluble CdSe QDs solution to accomplish binding process [34,35]. Obviously, both of the two synthetic routes are complicated and tedious. What's worse, oil soluble CdSe QDs are typically required for the self-assembly processes. In contrast, to synthesize water soluble CdSe QDs capped with mercaptan acid directly and then attach CdSe QDs to TiO_2 powder is a wise method to construct CdSe QDs-TiO_2 nanocomposites. It has a lot of incomparable advantages such as avoiding the use of organometallic precursors and organic ligands, low cost and environmental friendliness, mild reaction conditions, facile preparation procedures and so on.

In this study, we report this novel and green linker-assisted hybridization method to synthesize CdSe QDs-modified TiO_2. Water soluble CdSe QDs capped by mercaptoacetic acid (MAA) was firstly synthesized. Then CdSe QDs-modified TiO_2 nanoparticles were obtained by impregnating TiO_2 into as-synthesized CdSe QDs solution. Our results demonstrated that the CdSe QDs-modified TiO_2 showed greatly enhanced visible light photocatalytic activity. The role of quantum size effect of CdSe QDs in enhancing photocatalytic properties of CdSe QDs-modified TiO_2 was discussed in detail.

2. Experimental

2.1. Materials

$CdCl_2{\cdot}2.5\ H_2O$ (99.99%), sodium borohydride ($NaBH_4$) and sodium hydroxide (NaOH) were analytical grade and purchased from the Shanghai Chemical Co. Selenium powder (Se, 99%) and mercaptoacetic acid (MAA) was supplied by Aladdin-reagent. Malachite green (MG) was purchased from Sigma Aldrich (St. Louis, MO, USA). Commercial TiO_2 (P25: 80% anatase, 20% rutile; 50 $m^2\ g^{-1}$) was kindly supplied by Degussa Company. Commercial bulk CdSe powder was obtained from Alfa Aesar Company. Horseradish peroxidase (POD) and *N*, *N*-diethyl-*p*-phenylenediamine (DPD) were purchased from J&K Chemical Ltd. 5,5-Dimethyl-1-pyrroline-*N*-oxide (DMPO) was obtained from Sigma Co., Ltd. Terephthalic acid (TA) was from Acros Chemical Co. All chemicals were used without further purification and all experiments were carried out using deionized water.

2.2. Sample Preparation

2.2.1. Preparation of water soluble CdSe QDs

Water soluble CdSe QDs was prepared by the reaction between Cd^{2+} and NaHSe solution in the presence of MAA as a stabilizer, according to the literature reported by Rogach et al. [36] but with some modifications. Typically, 2 mmol of $CdCl_2{\cdot}2.5\ H_2O$ was dissolved in 200 mL of deionized water in a three-necked flask and deaerated with N_2 bubbling for 1 h. A proper amount of stabilizer (MAA) was then added to the above solution. The pH value of the solution was adjusted to 7 with 1 M NaOH aqueous solution. Oxygen-free NaHSe solution was prepared by mixing a certain amount of Se powder and $NaBH_4$ into 5 mL of deionized water. Then the freshly prepared oxygen-free NaHSe solution was quickly injected into the N_2 saturated Cd^{2+} solution under vigorous stirring. The initial molar ratio of Cd^{2+}:Se^{2-}:MAA was 3:2:5. After refluxing at 80 °C for 4 h, the desired orange–red CdSe QDs solution was obtained. In addition, equal volume of ethanol was added into the above solution to precipitate CdSe QDs. The precipitated CdSe QDs powder was separated by centrifugation, further washed with water and ethanol for several times, and dried in vacuum at 60 °C.

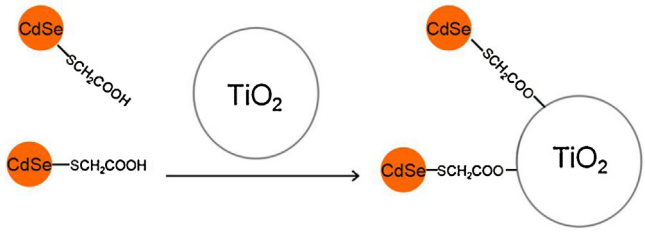

Scheme 1. Schematic of the formation process of CdSe QDs-modified TiO_2 through linker-assisted hybridization method.

2.2.2. Preparation of CdSe QDs-modified TiO_2

CdSe QDs-modified TiO_2 were prepared through a linker-assisted hybridization process (see Scheme 1) in aqueous solution. As our CdSe QDs was capped with MAA, the mercapto group (—SH) is conjugated on the surface of CdSe QDs, while the carboxylate group (—COOH) is ionized in water to make CdSe QDs water soluble. Because TiO_2 has a strong affinity for the carboxylate group (—COOH) [37], attachment of CdSe QDs to TiO_2 could be realized through hybridization process by MAA, the stabilizer of CdSe QDs, a bifunctional linker molecule.

The specific synthesis procedure was described as follows: 1.0 g of commercial TiO_2 (P25) powder was added into the appropriate volume of CdSe QDs solution and stirred for 24 h. The final products were centrifuged and washed with deionized water and ethanol for several times, and finally dried in vacuum at 60 °C for several hours. CdSe QDs-modified TiO_2 with different mass ratios of CdSe QDs to TiO_2 from 0.1% to 2.0% were prepared by following a similar procedure.

2.2.3. Preparation of bulk CdSe-modified TiO_2 and $TiO_{2-x}N_x$

As comparison, 0.01 g of commercial CdSe powder was added into TiO_2 suspensions formed by dispersing 1.0 g of TiO_2 powder into 200 mL of H_2O under stirring for 24 h. After centrifugation and fine grinding, the 1.0% bulk CdSe-modified TiO_2 was obtained. Additionally, N-doped TiO_2 was synthesized by traditional method [38], which was designated as $TiO_{2-x}N_x$.

2.3. Characterization

The crystal structures of samples were determined by using a Bruker D8 Advance X-ray diffractometer (XRD) at 40 kV and 40 mA with Ni-filtered Cu $K\alpha$ radiation in the 2θ ranging from 10° to 80° with a scan rate of 0.02° s^{-1}. The optical properties of the samples were characterized by a Cary 500 Scan UV–vis–NIR spectrometer with $BaSO_4$ as the background ranging from 200 to 800 nm. Edinburgh FL/FS900 fluorescence spectrometer was used to investigate the photoluminescence (PL) spectra for samples. The transmission electron microscope (TEM), high-resolution transmission electron microscope (HRTEM) and energy dispersive X-ray spectroscopy (EDX) were recorded on a FEI Tecnai G2 F20 instrument operated at an accelerating voltage of 200 kV. X-ray photoelectron spectroscopy (XPS) spectra were acquired using an ESCALAB 250 photoelectron spectrometer (Thermo Fisher Scientific) at 3.0×10^{-10} mbar with monochromatic Al $K\alpha$ radiation (E = 1486.2 eV). All of the binding energies were calibrated by the C 1s peak at 284.6 eV. The photoelectrochemical analysis was carried out in a conventional three-electrode cell filled with 0.1 M of Na_2SO_4 electrolyte (30 mL). The sample was deposited on a sheet of indium-tin-oxide (ITO) glass to serve as the working electrode with 0.5 cm × 0.5 cm area. The photocurrent measurements were measured on an electrochemical workstation (CHI-660D, China). The

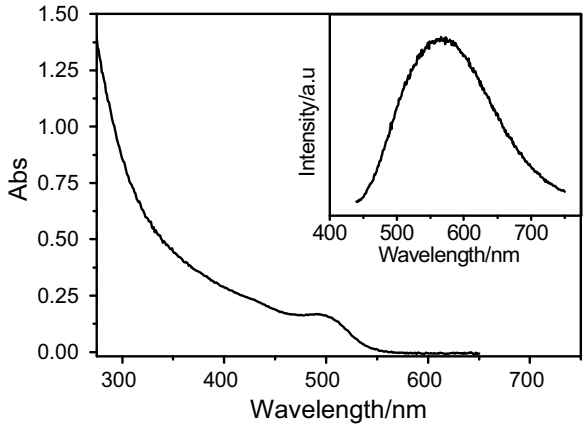

Fig. 1. UV–vis absorption and PL spectra of water soluble CdSe QDs solution prepared at 80 °C for 4 h.

Mott–Schottky experiments were conducted on a Precision PARC workstation. Electron paramagnetic resonance (EPR) was used to detect radicals spin-trapped by 5, 5-dimethyl-1-pyrroline-*N*-oxide (DMPO). The signals were collected by a Bruker model A300 spectrometer (Bruker Instruments, Inc.) with the settings of center field (3512 G), microwave frequency (9.86 GHz), and power (20 mW).

2.4. Test of photocatalytic activity

The photocatalytic degradation of MG was conducted in an aqueous solution. The system was cooled by fan to maintain at room temperature. The visible light source was a 500 W Xe-arc lamp (CEL-S500 Beijing China Education Au-light Co., Ltd.) with a 420–800 nm band-pass filter. A total of 40 mg of photocatalyst was added to 80 mL of MG solution (10 mg/L, 10 ppm) contained in a 100-mL Pyrex glass vessel. Prior to irradiation, the suspensions were magnetically stirred in dark for 2 h in order to reach adsorption–desorption equilibrium between the catalyst and MG. At given time intervals, 3 mL of suspensions were sampled and centrifuged to remove the catalyst. The degraded solutions were analyzed using a Varian Cary 50 Scan UV–vis spectrophotometer, and the absorption peak at 616 nm was monitored. This peak was used to assess the effect of the photocatalysis for the degradation of MG.

3. Results and discussion

3.1. Characterization

3.1.1. UV–vis absorption and photoluminescence spectra of CdSe QDs aqueous solution

The UV–vis absorption and PL spectra measurements were employed to characterize CdSe QDs aqueous solution. As shown in Fig. 1, the CdSe QDs displays an excitonic absorption peak at wavelength of about 500 nm, which is obviously blue shifted as compared to bulk CdSe. The peak is attributed to the 1s-1s electronic transition for the first excitonic state of quantum-sized CdSe [36] with band gap of 2.55 eV. The inset of Fig. 1 shows that CdSe QDs has a PL spectrum ranging from 450 nm to 750 nm. This broad PL spectrum also shows a nonzero tail toward longer wavelength, indicating the presence of surface energy traps [39]. These results indicate that water soluble CdSe QDs has been successfully synthesized, which lays the foundation for the following synthesis of CdSe QDs-modified TiO_2.

3.1.2. Light absorption properties of CdSe QDs and CdSe QDs-modified TiO_2

As far as we know, the light absorption property of photocatalyst plays a vital role in the photocatalytic process. The inset of Fig. 2a shows band gap energy (E_g) of CdSe QDs powder by using the method of Li et al., which depends on the equation of $[F(R)E]^2 = A(E - E_g)$ [40]. The band gap value is approximately 2.21 eV as compared to 1.75 eV of bulk CdSe. There is an obvious band gap enlargement due to quantum size effect. It should be noted that the absorption edge of CdSe QDs powder (band gap of 2.21 eV, shown in Fig. 2) exhibits a slight red shift compared to CdSe QDs in water phase (band gap of 2.55 eV, shown in Fig. 1). This indicates that the crystal size of the former is slightly larger than that of the latter, which can be attributed to the growth or aggregation of CdSe QDs during the vacuum drying process. Despite this, the crystal size of CdSe QDs is still rather small (~4 nm) and an evident quantum size effect can be observed. The UV–vis diffuse reflectance absorption spectra $F(R)$ of pure TiO_2, bulk CdSe-modified TiO_2 and CdSe QDs-modified TiO_2 are shown in Fig. 2b. As can be seen, pure TiO_2 nanoparticles has a strong absorption in the UV light region and exhibits the fundamental absorption edge corresponding to the band gap energy of 3.2 eV. When TiO_2 is modified with bulk CdSe, it displays the characteristic absorption of bulk CdSe in visible region. It can also be seen that the absorption edge of CdSe QDs-modified TiO_2 in visible light region is consistent with that of pure CdSe QDs, owing to the successful introduction of CdSe QDs.

3.1.3. XRD patterns of CdSe QDs and CdSe QDs-modified TiO_2

XRD analysis was used to investigate the phase structures of the samples. As shown in Fig. 3a, the CdSe QDs has a crystalline structure of face-centered cubic CdSe according to JCPDS 19-0191. The obviously broadened diffraction peak indicates that the size of CdSe QDs is very small. The average crystallite size is about 4.5 nm as determined by the Debye–Scherrer equation. Fig. 3b shows the XRD patterns of the CdSe QDs-modified TiO_2 samples. It is found that the samples are all well-crystallized. The XRD diffraction peaks at around 2θ values of 25.3° 37.8°, 48.0°, 53.9° and 55.1° can be indexed to the (1 0 1), (0 0 4), (2 0 0), (1 0 5) and (2 1 1) crystallographic planes of anatase TiO_2 (JCPDS 21-1272). The peak at around 2θ value of 27.4° can be attributed to the (1 1 0) crystallographic plane of rutile TiO_2 (JCPDS 21-1276). All of the X-ray diffraction peaks are indexed to TiO_2, indicating that the introduction of CdSe QDs does not change the lattice structure of TiO_2. Moreover, no diffraction peaks assigned to CdSe QDs are found, which could be ascribed to the small amount of CdSe QDs (max 2.0 wt%) and their highly dispersion in TiO_2 [41].

3.1.4. TEM and HRTEM images of CdSe QDs-modified TiO_2

The morphology and microstructure of CdSe QDs and 1.0% CdSe QDs-modified TiO_2 were revealed by TEM combined with EDX spectroscopy. Well dispersed CdSe QDs particles with diameters of about 3 nm can be clearly seen in Fig. 4a. The lattice spacing measured for this crystalline plane is 0.351 nm, corresponding to the (1 1 1) plane of cubic CdSe (JCPDS 19-0191). After modifying TiO_2 with CdSe QDs, small crystallites with sizes of several nanometers are clearly seen on the surface of TiO_2 (Fig. 4b). As observed by HRTEM image (Fig. 4c), the lattice spacings of the small crystallites are detected to be 0.351 nm and 0.215 nm, corresponding to (1 1 1) and (2 2 0) planes of cubic CdSe (JCPDS 19-0191), respectively. Meanwhile, the lattice spacings of 0.352 nm and 0.189 nm belong to the (1 0 1) and (2 0 0) planes of anatase TiO_2 (JCPDS 21-1272), respectively. The EDX spectroscopy has also been performed. As shown in Fig. 4d, the elements of Ti, O (coming from TiO_2) and Se, Cd, S (coming from MAA-capped CdSe QDs) are detected in CdSe

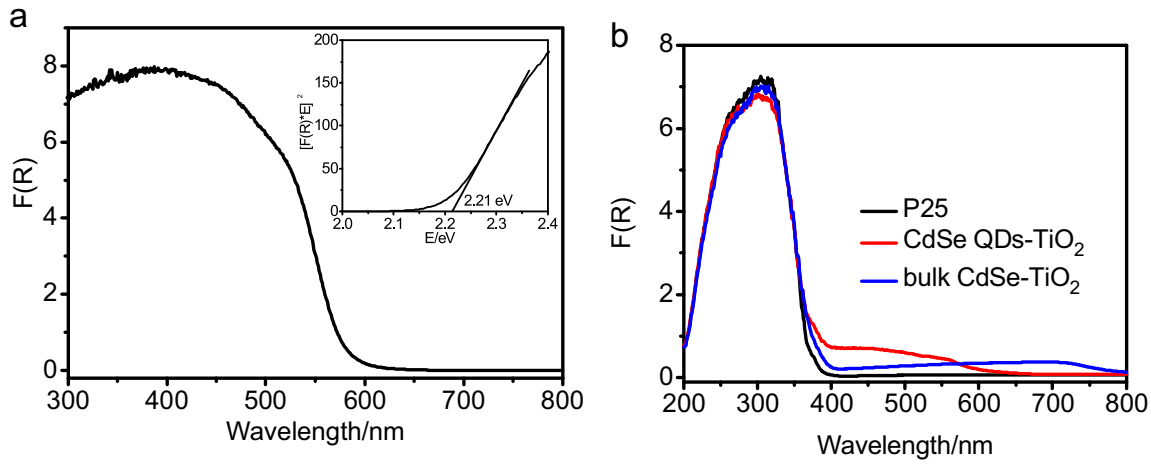

Fig. 2. UV–vis diffuse reflectance absorption spectra $F(R)$ of CdSe QDs (a), pure TiO_2, bulk CdSe-modified TiO_2 and CdSe QDs-modified TiO_2 (b); the optical band gap energy (E_g) of CdSe QDs (inset of (a)).

QDs-modified TiO_2. Therefore, the structure of CdSe QDs-modified TiO_2 is confirmed.

3.1.5. High resolution XPS spectra of CdSe QDs-modified TiO_2

X-ray photoelectron spectroscopy (XPS) was carried out to determine the chemical composition of the 1.0% CdSe QDs-modified TiO_2 and the valence states of various species presented therein. As shown in Fig. 5a, the C 1s high resolution spectra of the sample can be deconvoluted into four peaks corresponding to C—C, C—OH, C═O and HO—C═O, with binding energy of 284.6 eV, 286.2 eV, 287.6 eV and 288.6 eV, respectively [37,42]. The carbon species arise from the adventitious carbon, CO_2 adsorption and carboxylic acid groups of bifunctional linker MAA. From Fig. 5b, the Ti 2p core level spectrum can be observed at binding energies around 459.5 eV (Ti $2p_{3/2}$) and 464.95 eV (Ti $2p_{1/2}$), which is in good agreement with that in TiO_2 [43]. The two strong peaks at 405.82 eV and 412.15 eV correspond to the binding energies of Cd $3d_{5/2}$ and Cd $3d_{3/2}$ respectively (Fig. 4c) and peak at 54.06 eV corresponds to the binding energy of Se 3d (Fig. 4d). It is worth noting that the peak at about 59 eV corresponding to selenium oxide is ascribed to the partial oxidization of CdSe, because the surface of CdSe QDs is prone to be oxidized in air [44]. Therefore, XPS spectra of CdSe QDs-modified TiO_2 demonstrate that CdSe QDs has already been modified onto TiO_2 successfully through bifunctional linker MAA and formed CdSe QDs-modified TiO_2, except for the partial oxidization of CdSe QDs inevitably.

3.2. Evaluation of photocatalytic activity

3.2.1. Enhanced photocatalytic activity of CdSe QDs-modified TiO_2 for MG degradation

Malachite green (MG), which shows an absorption maximum at 616 nm [45], is chosen as a representative organic dye to evaluate the photocatalytic activities of our samples. The degradation efficiencies of MG over pure TiO_2 and CdSe QDs-modified TiO_2 with different mass ratios of CdSe QDs to TiO_2 are displayed in Fig. 6a. All the CdSe QDs-modified TiO_2 samples exhibit much higher photocatalytic activities than pure TiO_2. With the content of CdSe QDs increases from 0.1% to 1.0%, the photocatalytic activity of CdSe QDs-modified TiO_2 increases obviously. However, when the loading amount of CdSe QDs exceeds 1.0%, the photocatalytic activity starts to decrease as the content of CdSe QDs increases. The content of CdSe QDs is pivotal for photocatalytic activity of CdSe QDs-modified TiO_2. Suitable content of CdSe QDs can lead to both excellent visible light absorption and well particle dispersion on the TiO_2 surface, and therefore are beneficial for high activity. However, too higher content of CdSe QDs would form overlapping agglomerates on the TiO_2 surface and lower the activity for MG photodegradation. The optimal loading amount of CdSe QDs on TiO_2 for improving the

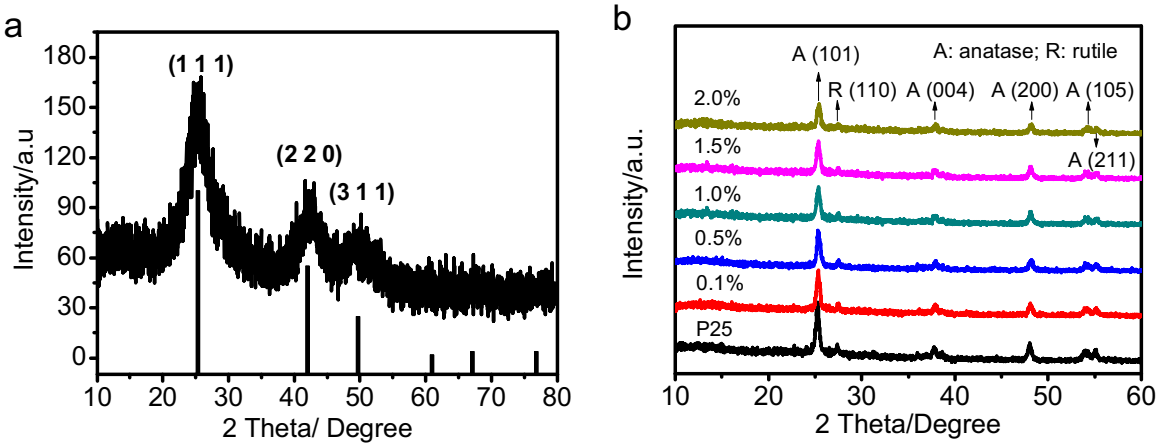

Fig. 3. XRD patterns of CdSe QDs powder (a) and CdSe QDs-modified TiO_2 with different mass ratios of CdSe QDs to TiO_2 (b).

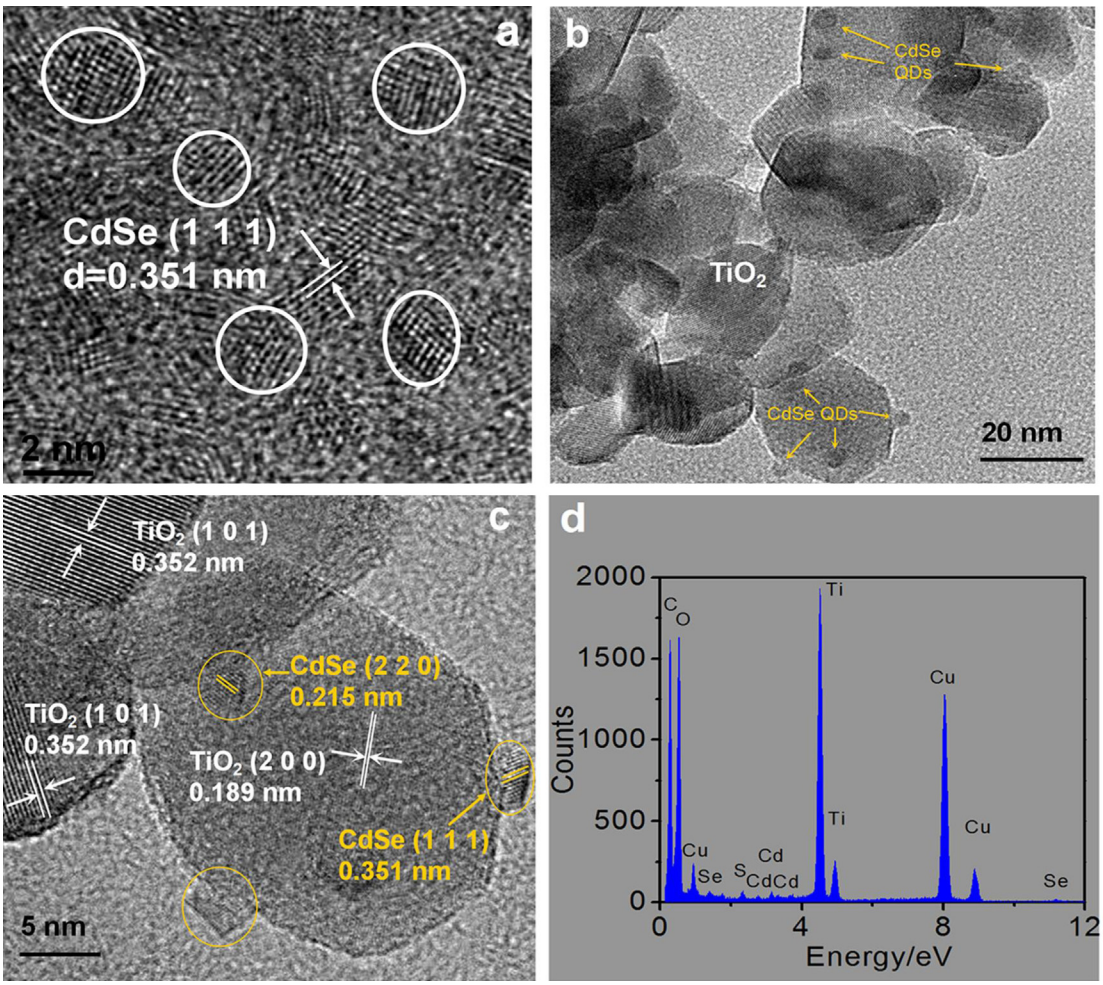

Fig. 4. The HRTEM image of CdSe QDs (a); TEM (b), HRTEM image (c) and EDX patterns (d) of CdSe QDs-modified TiO_2.

photocatalytic property is 1.0%. It should be noted that the best-performing sample (1.0% CdSe QDs-modified TiO_2) is selected as a model for the follow-up study.

The photocatalytic degradation efficiencies of MG over different samples are displayed in Fig. 6b and Fig. S1. The blank test shows that MG is only slightly degraded without catalysts, indicating the photolysis of MG can be ignored. Under visible light irradiation for 6 h, 6.8% and 56.2% of MG can be degraded by TiO_2 and CdSe QDs, respectively. This result indicates that the photosensitization of MG is very weak and the visible light absorption of MG has little influence on the evaluation of real photocatalytic activity of photocatalyst. In comparison, 97.6% of MG can be degraded by CdSe QDs-modified TiO_2. Although CdSe QDs can absorb visible light (shown in Fig. 2a), the high recombination rate of photo-generated electron–holes leads to a lower activity. For CdSe QDs-modified TiO_2, the photoresponse is extended into visible region (shown in Fig. 2b). Moreover, high separation efficiency of photo-generated electron–holes can be achieved due to the electron transfer from CdSe QDs into TiO_2. As a result, CdSe QDs-modified TiO_2 exhibits greatly enhanced activities than both TiO_2 and CdSe QDs. To further investigate its outstanding activity, $TiO_{2-x}N_x$ was also used as a reference catalyst. Remarkably, CdSe QDs-modified TiO_2 exhibits much higher activity than $TiO_{2-x}N_x$. As shown in Fig. S2a, the photodegradation process could be assigned to a pseudo-first-order kinetics by linear transforms $-\ln(C/C_0) = kt$, where C_0 is the adsorption equilibrium concentration of MG, and C is the concentration of MG at given time t. The apparent rate constants (k) are clearly seen in Fig. S2b. The k value of CdSe QDs-modified TiO_2 ($0.6196\,h^{-1}$) is about 4.6 times larger than that of $TiO_{2-x}N_x$ ($0.1379\,h^{-1}$). In addition, CdSe QDs displays much higher activity ($k = 0.1379\,h^{-1}$) than bulk CdSe ($k = 0.0219\,h^{-1}$) which has nearly no activity. This is because CdSe QDs possesses an enlarged band gap and stronger redox ability than bulk CdSe due to quantum size effect.

Particularly, CdSe QDs-modified TiO_2 exhibits much higher activity than bulk CdSe-modified TiO_2. The k value of the former one ($0.6196\,h^{-1}$) is about 7.2 times larger than that of the latter one ($0.0857\,h^{-1}$). The enhanced activities could be mainly attributed to two reasons. On the one hand, large grain sizes of bulk CdSe will lead to deficient contact between CdSe and TiO_2 and weak interactions, while quantum-sized CdSe can be highly dispersed in TiO_2 and has strong interactions with TiO_2 via bifunctional linker. On the other hand, the quantum size effect of CdSe QDs plays a crucial role in enhancing photocatalytic activities of CdSe QDs-modified TiO_2, which will be discussed in detail in Section 3.3.

In addition, p-hydroxyazobenzene (p-HAB), whose absorption peak is at 347 nm, is also used as model pollutant to evaluate the activity of our photocatalyst. A 500 nm cut-off filter is placed on the back of 420–800 nm band-pass filter to obtain the visible light source ($500\,nm < \lambda < 800\,nm$). As p-HAB has no absorption in the visible region with $\lambda > 500$ nm, its degradation can completely exclude the photosensitized reaction of p-HAB. As shown in Fig. S3, after 6 h of irradiation, the peak of p-HAB reduces a lot. The corresponding photocatalytic conversion ratio is up to 65.2%. Therefore, we should conclude that the CdSe QDs-modified TiO_2

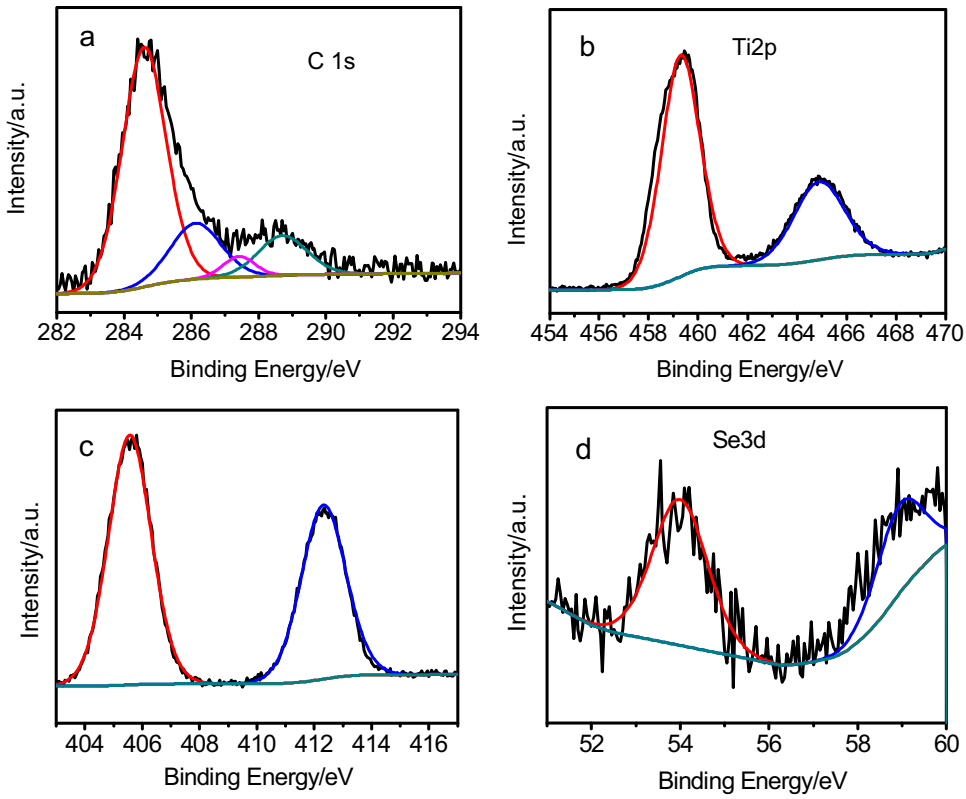

Fig. 5. High-resolution XPS spectra of the C 1s (a), Ti 2p (b), Cd 3d (c) and Se 3d (d) regions for the CdSe QDs-modified TiO_2.

can be photo-excited under visible light irradiation and generate the electron–holes pairs, which can participate in the photocatalytic process for organic pollutant degradation.

3.2.2. *Photocatalytic stability of CdSe QDs-modified TiO_2*

It is known that the photocorrosion or photodissolution might occur on the photocatalyst surface in the photocatalytic reaction, especially for sulfide such as CdS. So CdSe QDs-modified TiO_2 before and after photodegradation of MG are compared by XRD and XPS investigation. XRD analysis in Fig. S4 shows that the crystal structure of the photocatalyst does not change after the photocatalytic reaction. As can be seen from Fig. S5, the binding energy of Cd 3d has no obvious charge shift after the photodegradation of MG, indicating that the chemical valence state of Cd element does not change during the photocatalytic reaction process. Additionally, the decrease of Cd 3d intensity means that Cd^{2+} loss occurs after the photocatalytic reaction. Moreover, the photocatalytic reaction is carried out repeatedly for three times (shown in Fig. 7). The photocatalytic efficiency displays slight decrease. The loss in activity after recycling the catalyst could be related to the difficulty in recovering nanoparticles and photocorrosion of the CdSe QDs. And this is the main obstacle that hinders metal sulfide and selenide from application in photocatalytic field. Even so, the fact that modification of CdSe QDs enhances the visible light photocatalytic activity of TiO_2 has achieved our research target.

3.3. *The role of quantum size effect in CdSe QDs-modified TiO_2 photocatalyst*

As displayed in Section 3.1, CdSe QDs was hybridized with TiO_2 nanoparticles and the CdSe QDs-modified TiO_2 was synthesized successfully. Besides, the photocatalytic degradation experiments

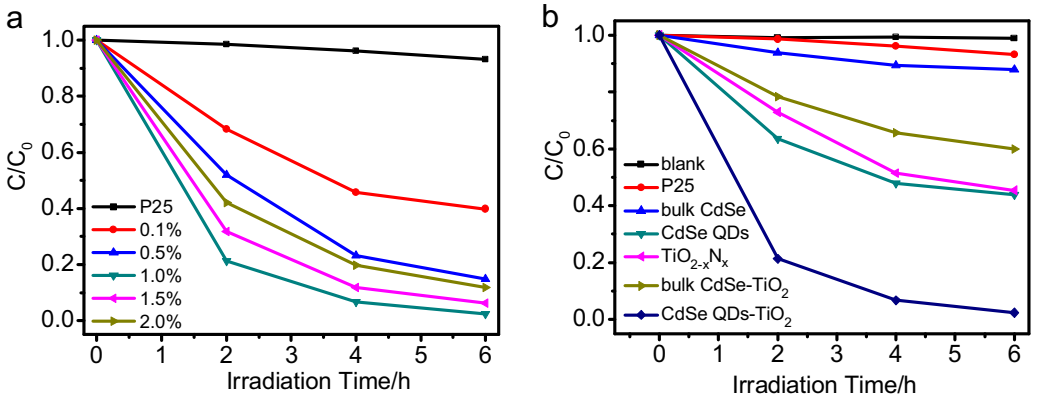

Fig. 6. Photocatalytic degradation of MG aqueous solution for TiO_2 and CdSe QDs-modified TiO_2 different mass ratios of CdSe QDs to TiO_2 (a); blank (without catalyst), TiO_2, bulk CdSe, CdSe QDs, $TiO_{2-x}N_x$, bulk CdSe-modified TiO_2 and CdSe QDs-modified TiO_2 (b).

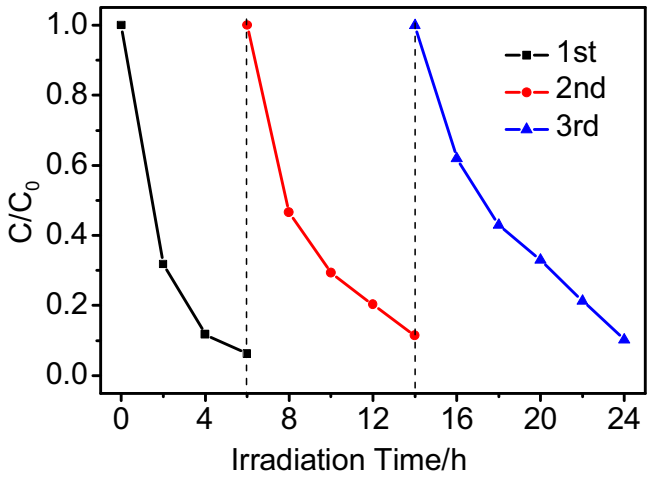

Fig. 7. Photocatalytic degradation stability of MG over CdSe QDs-modified TiO_2 for three times under visible light irradiation.

revealed that CdSe QDs-modified TiO_2 exhibited much higher activities than both pure TiO_2 powder and bulk CdSe-modified TiO_2. Then what advantage does quantum-sized CdSe possess compared with bulk CdSe? What specific role does CdSe QDs play in the photocatalytic degradation process over CdSe QDs-modified TiO_2? The questions proposed above will be discussed in the following section.

3.3.1. More negative conduction band potentials of CdSe QDs

Electrochemical analysis was carried out to investigate the electronic properties of samples. Fig. 8 displays the capacitance measurement in the Mott–Schottky-type plot for CdSe QDs, bulk CdSe and TiO_2. All samples are n-type semiconductors because of the positive slopes of the C^{-2}–E plots [46]. Another important parameter derived from the measurement is the flat band potential [47]. It can be obtained from Fig. 8 that the flat band potentials (V_{fb}) of bulk CdSe and TiO_2 are −0.68 V and −0.54 V vs. Ag/AgCl, corresponding to −0.48 V vs. normal hydrogen electrode (NHE) for bulk CdSe and −0.34 V vs. NHE for TiO_2 [48], respectively. For n-type semiconductors, the conduction band potentials (V_{CB}) are very close (more negative by ~−0.1 V) to their flat band potentials [49]. Thereby, the V_{CB} of bulk CdSe and TiO_2 are about −0.58 V and −0.44 V vs. NHE, respectively, and both of them are more negative than the standard redox potential of $O_2/O_2^{\bullet-}$ (−0.33 V vs. NHE) [50]. Besides, the photo-generated electrons of bulk CdSe are prone to transfer to the conduction band of TiO_2 because of the more negative V_{CB} of bulk CdSe than that of TiO_2. The valence band potentials (V_{VB}) of bulk CdSe and TiO_2 are about 1.17 V and 2.76 V vs. NHE, respectively, according to the formula $E_g = V_{VB} - V_{CB}$. As for as-prepared CdSe QDs, the flat band potentials is about −0.89 V vs. Ag/AgCl according to Fig. 8. Similarly, it can be deduced that the V_{CB} of CdSe QDs is about −0.79 V vs. NHE, which is more negative than that of bulk CdSe obviously because of the quantum size effect of CdSe QDs. As the CdSe QDs has a band gap of 2.21 eV (as represented in Fig. 2a), the V_{VB} of CdSe QDs is about 1.42 V vs. NHE. In order to be seen clearly, the V_{fb}, V_{CB} and V_{VB} of all samples are summarized and shown in Table 1.

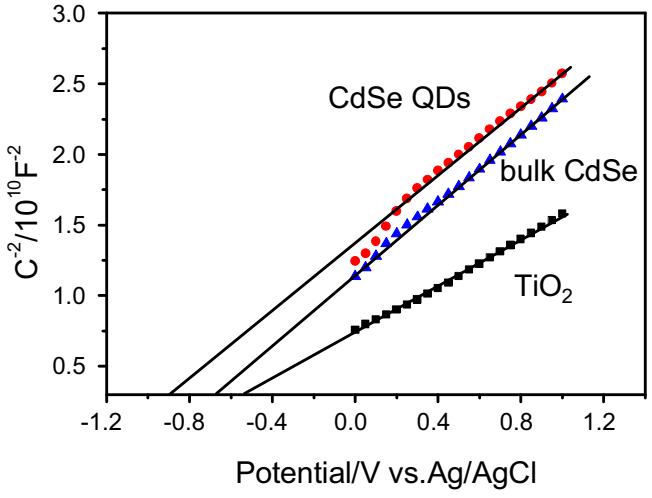

Fig. 8. Mott–Schottky plots of CdSe QDs, bulk CdSe and TiO_2 electrodes in 0.1 M Na_2SO_4 aqueous solution at pH = 7. Counter electrode: Pt. Reference electrode: Ag/AgCl. Electrolyte: 0.1 M Na_2SO_4 (30 mL). Frequency: 1 kHz.

Table 1
The flat band, conduction and valence band potentials of TiO_2, bulk CdSe and CdSe QDs.

Sample	CdSe QDs (V)	Bulk CdSe (V)	TiO_2 (V)
V_{fb} vs. Ag/AgCl	−0.89	−0.68	−0.54
V_{fb} vs. NHE	−0.69	−0.48	−0.34
V_{CB} vs. NHE	−0.79	−0.58	−0.44
V_{VB} vs. NHE	1.42	1.17	2.76

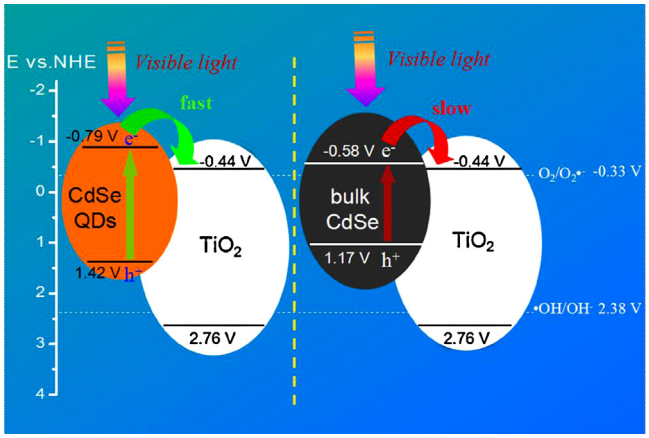

Scheme 2. Illustrations of the energy band positions of CdSe QDs, bulk CdSe, and TiO_2 and the photo-generated electron transfer process in the CdSe QD-modified TiO_2 system (left) and bulk CdSe-modified TiO_2 system (right) under visible light irradiation.

3.3.2. Stronger driving forces for electron transfer and enhanced separation efficiency of electron–holes

As far as we know, a necessary step for semiconductor photocatalytic reaction is the generation and separation of electron–hole pairs [51]. The transfer of electrons in the photocatalytic process is very important, which would inhibit the recombination of electrons and holes and increase the activity. According to the experimental results of flat band potential test, the energy band positions of CdSe QDs, bulk CdSe, and TiO_2 and electron transfer process in CdSe–TiO_2 system can be illustrated in Scheme 2. Under visible light irradiation, the photoelectrons will be generated in conduction band of CdSe in both CdSe QDs-modified TiO_2 and bulk CdSe-modified TiO_2 system. Then the photo-generated electrons will transfer to the conduction band of TiO_2 because the V_{CB} of both bulk CdSe and CdSe QDs are more negative than that of TiO_2. However, the transfer rates are different. The driving force for electron transfer from CdSe to TiO_2 is determined by the energy difference between the two conduction band positions. CdSe QDs with its more negative V_{CB} is expected to have much stronger driving forces for injecting electrons from CdSe into TiO_2 [52]. As a result, the electron transfer

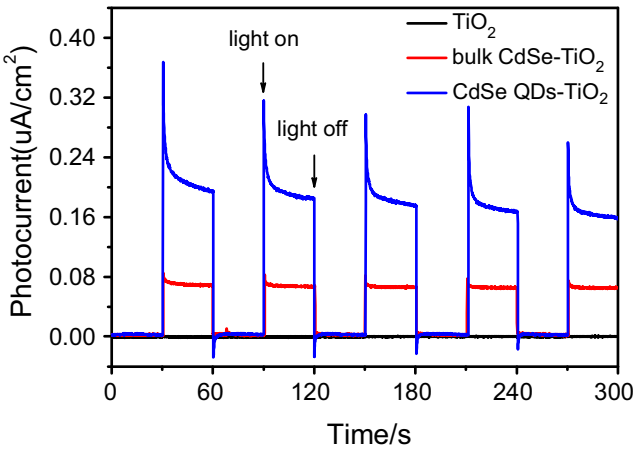

Fig. 9. Photocurrent spectra of CdSe QDs-modified TiO_2, bulk CdSe-modified TiO_2 and TiO_2 under visible light irradiation.

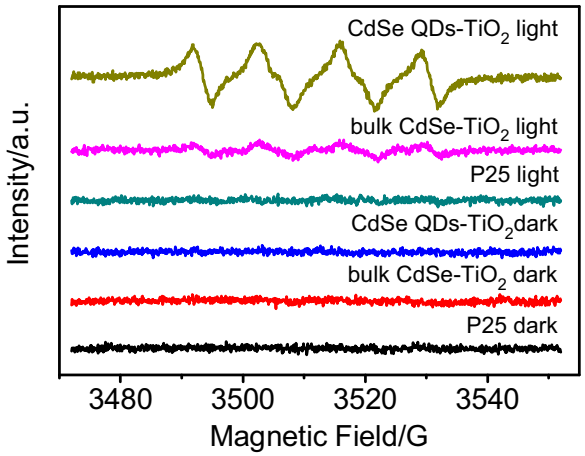

Fig. 11. DMPO spin-trapping EPR spectra of TiO_2 (a), bulk CdSe-modified TiO_2 (b) and CdSe QDs-modified TiO_2 (c) in methanol dispersion for DMPO–O_2•$^-$ in dark or under visible light irradiation.

rate from CdSe QDs to TiO_2 is much faster than that from bulk CdSe to TiO_2 (as illustrated in Scheme 2), which would be beneficial for an efficient charge carrier's separation.

To our knowledge, the photocurrent response has been demonstrated to be a useful technique for investigating the separation efficiency of photogenerated electron–hole pairs [53]. The photocurrent–time (I–t) profiles with zero bias electrode potential are shown in Fig. 9. As for CdSe–TiO_2 nanocomposites (CdSe QDs-modified TiO_2 and bulk CdSe-modified TiO_2), the interactions between CdSe and TiO_2 form heterostructures and facilitate the interfacial electron transfer, generating evident photocurrent under visible light irradiation. Furthermore, the much higher photocurrent response suggests the more efficient separation of photo-generated electron–hole pairs of CdSe QDs-modified TiO_2 than that of bulk CdSe-modified TiO_2.

3.3.3. *More quantities of active species generated during the photocatalytic process*

It is known that the photocatalytic degradation of organic pollutants under visible light irradiation is mainly due to some active species, such as O_2•$^-$, H_2O_2, •OH, holes and so on. To investigate the role of these active species, different types of scavengers were added in the photocatalytic degradation process. Fig. 10 shows the photocatalytic activity of CdSe QDs-modified TiO_2 toward the degradation of MG under different conditions. Without the addition of scavengers, the photocatalytic conversion ratio of MG degradation is 93.8% after 6 h of visible light irradiation. When 0.1 g of ammonium oxalate (AO) as a hole-scavenger [54] is added into the reaction system, the degradation ratio of MG decreases obviously, suggesting that the photo-generated holes play an important role in the photocatalytic reaction. After 2 mL of *tert*-butyl alcohol (TBA) as a scavenger for •OH [55] is added in the system, the degradation ratio is also decreased. Benzoquinone (BQ) has the ability to trap O_2•$^-$ by a simple electron transfer mechanism [56]. As shown in Fig. 10, the addition of BQ (1 mg) leads to the most inhibition of the MG degradation, indicating that O_2•$^-$ plays the most important role in the photocatalytic process. Moreover, dissolved O_2 as an efficient electron scavenger also promotes the degradation process. Based on the above analysis, it can be concluded that the degradation of MG is driven mainly by O_2•$^-$. Meanwhile, •OH and holes also promote the process of photocatalytic reaction. The following experiments also demonstrated that more quantities of active species were produced in CdSe QDs-modified TiO_2 system than that in bulk CdSe-modified TiO_2 system due to quantum size effect.

To confirm and analyze O_2•$^-$ radicals, EPR spin-trap with DMPO technique [57] was employed in this experiment. As shown in Fig. 11, DMPO–O_2•$^-$ adducts with six characteristic peaks are observed obviously for CdSe QDs-modified TiO_2 and bulk

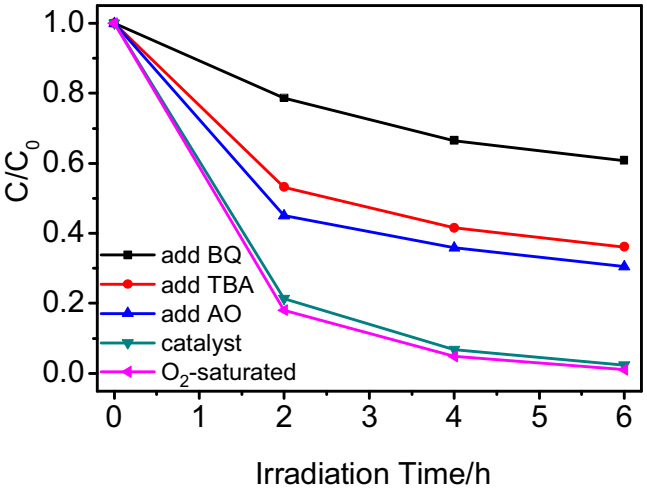

Fig. 10. Photocatalytic degradation of MG over CdSe QDs-modified TiO_2 under different conditions with exposure to visible light.

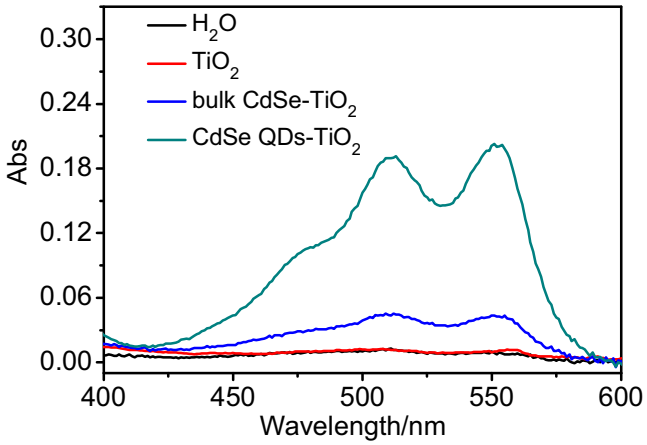

Fig. 12. Detection of H_2O_2 in TiO_2, bulk CdSe-modified TiO_2 and CdSe QDs-modified TiO_2 water dispersions by addition of DPD and POD to the dispersions after 2 h of visible light irradiation.

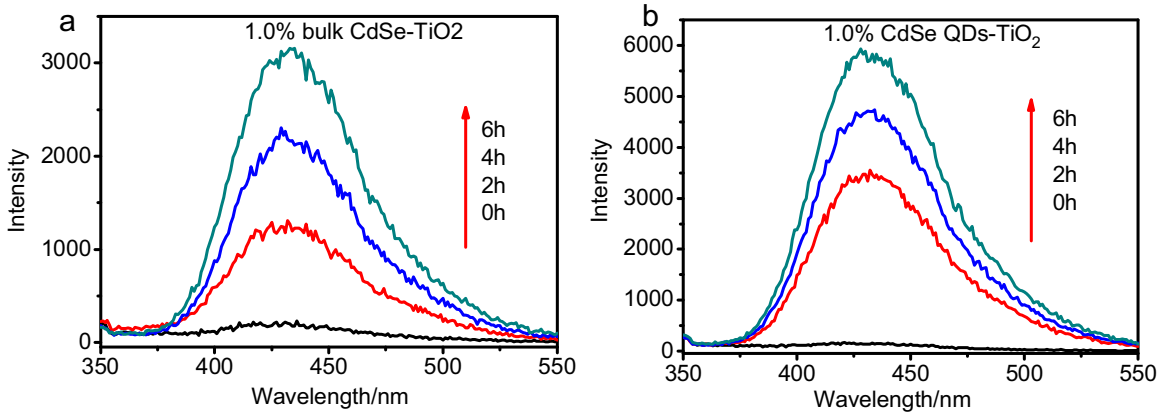

Fig. 13. •OH-trapping PL spectra of bulk CdSe-modified TiO_2 (a) and CdSe QDs-modified TiO_2 (b) in TA solution under visible light irradiation for 6 h.

CdSe-modified TiO_2 under visible light irradiation, while in dark there are no obvious peaks observed. As for TiO_2, no distinct peaks are detected whether in dark or under visible light irradiation. This manifests that $O_2\bullet^-$ is one of the main active species during the photocatalytic degradation process upon MG over both CdSe QDs-modified TiO_2 and bulk CdSe-modified TiO_2. Notably, the intensity of DMPO–$O_2\bullet^-$ adducts for CdSe QDs-modified TiO_2 is much stronger than that of bulk CdSe-modified TiO_2, which was in accordance with the photocatalytic activity results. This indicates that much more $O_2\bullet^-$ are generated in CdSe QDs-modified TiO_2 system under visible light irradiation. We hold the opinion that this phenomenon is closely related with the quantum size effect of CdSe QDs. First, the V_{CB} of CdSe QDs (−0.79 V) is more negative than that of bulk CdSe (−0.58 V) (illustrated in Scheme 2), resulting in much stronger reduction ability of photo-generated electrons. As $O_2\bullet^-$ is formed by the reaction between photo-generated electrons and the absorbed O_2, larger amount of $O_2\bullet^-$ will be produced in CdSe QDs-modified TiO_2. Second, in comparison with bulk CdSe-modified TiO_2 system, the electron transfer rate from CdSe QDs to TiO_2 is much faster (illustrated in Scheme 2) and more electrons will be transferred into the conduction band of TiO_2 followed by reacting with the absorbed O_2. Consequently, more $O_2\bullet^-$ are produced in CdSe QDs-modified TiO_2.

The DPD method [58] was employed for the detection of H_2O_2, which is another important intermediate species in the photocatalytic reaction. As shown in Fig. 12, in the presence of either CdSe QDs-modified TiO_2 or bulk CdSe-modified TiO_2 under visible light irradiation for 2 h, two obvious peaks with absorption maxima at about 510 nm and 551 nm are observed clearly, indicating the formation of H_2O_2 [58]. While for water and TiO_2, there are no obvious peaks observed under the same conditions. So it can be inferred that H_2O_2 is actually generated due to the introduction of CdSe into TiO_2. What's more, the significant difference of intensity demonstrates that more H_2O_2 are produced in CdSe QDs-modified TiO_2 than in bulk CdSe-modified TiO_2.

As displayed in Table 1 and Scheme 2, both of the valence band potentials of CdSe QDs (1.42 V vs. NHE) and bulk CdSe (1.17 V vs. NHE) are more negative than the standard redox potential of •OH/OH^- (2.38 V vs NHE), indicating that the photo-generated holes in VB of CdSe cannot oxidize H_2O to give •OH. However, •OH can be obtained from reaction between H_2O_2 and electrons [50]. Terephthalic acid photoluminescence (TA-PL) technique [59], as a very sensitive method to detect the formation of •OH radicals, was employed in our experiment. The intensity of the peak at around 426 nm, which is attributed to 2-hydroxyl-terephthalic acid (TAOH), is proportional to the amount of •OH radicals. So the quantity changes of •OH produced in the process can be detected through monitoring the photoluminescence intensity of TAOH. As can be seen in Fig. 13, the fluorescence intensities of both bulk CdSe–TiO_2–TA and CdSe QDs–TiO_2–TA solution increase with irradiation time, which means that •OH radicals are indeed generated under visible light irradiation. Obviously, the fluorescence intensity of CdSe QDs–TiO_2–TA solution is much stronger than that of bulk CdSe–TiO_2–TA solution. That is to say, much more •OH are generated during the photodegradation process of MG over CdSe QDs-modified TiO_2 than that over bulk CdSe-modified TiO_2, corresponding to the much enhanced photocatalytic activity.

4. Conclusions

In summary, we have successfully synthesized CdSe QDs-modified TiO_2 powders through a novel and green linker-assisted hybridization method. The as-prepared CdSe QDs exhibits obvious quantum size effect. Moreover, CdSe QDs has been successfully modified onto TiO_2 nanoparticles according to the TEM and XPS results. CdSe QDs-modified TiO_2 performs much better activity than both pure TiO_2 and bulk CdSe modified-TiO_2 toward degradation of MG under visible light irradiation. The quantum size effect leads to enlargement of its band gap (from 1.75 eV of bulk CdSe to 2.21 eV of CdSe QDs). In contrast with bulk CdSe-modified TiO_2, the larger difference between the conduction band potentials of CdSe QDs and TiO_2 can greatly increase the electron transfer rate from CdSe QDs to TiO_2, which would be beneficial for an efficient charge carrier's separation. Furthermore, our experiments also demonstrate that more quantities of active species ($O_2\bullet^-$, H_2O_2, •OH) are produced in CdSe QDs-modified TiO_2 system due to quantum size effect.

Acknowledgments

This work was financially supported by the NNSF of China (No: 21173047, 21073036 and 21373049) and the National Basic Research Program of China (973 Program, No: 2013CB632405).

Appendix A. Supplementary data

Supplementary material related to this article can be found, in the online version, at http://dx.doi.org/10.1016/j.apcatb.2014.05.032.

References

[1] N. Wang, L. Zhu, Y. Huang, Y. She, Y. Yu, H. Tang, J. Catal. 266 (2009) 199–206.
[2] X. Chen, S.S. Mao, Chem. Rev. 107 (2007) 2891–2959.

[3] S. Karvinen, R.-J. Lamminmäki, Solid State Sci. 5 (2003) 1159–1166.
[4] A. Kudo, Y. Miseki, Chem. Soc. Rev. 38 (2009) 253–278.
[5] H. Huang, D. Li, Q. Lin, W. Zhang, Y. Shao, Y. Chen, M. Sun, X. Fu, Environ. Sci. Technol. 43 (2009) 4164–4168.
[6] Y. Hu, D. Li, Y. Zheng, W. Chen, Y. He, Y. Shao, X. Fu, G. Xiao, Appl. Catal., B: Environ. 104 (2011) 30–36.
[7] J. Wang, H. Ruan, W. Li, D. Li, Y. Hu, J. Chen, Y. Shao, Y. Zheng, J. Phys. Chem. C 116 (2012) 13935–13943.
[8] Y. Zhang, L. Fei, X. Jiang, C. Pan, Y. Wang, J. Am. Ceram. Soc. 94 (2011) 4157–4161.
[9] I. Paramasivam, Y.-C. Nah, C. Das, N.K. Shrestha, P. Schmuki, Chem.—Eur. J. 16 (2010) 8993–8997.
[10] A.J. Nozik, M.C. Beard, J.M. Luther, M. Law, R.J. Ellingson, J.C. Johnson, Chem. Rev. 110 (2010) 6873–6890.
[11] S. Neeleshwar, C.L. Chen, C.B. Tsai, Y.Y. Chen, C.C. Chen, S.G. Shyu, M.S. Seehra, Phys. Rev. B: Condens. Matter 71 (2005) 201307.
[12] R.D. Schaller, J.M. Pietryga, V.I. Klimov, Nano Lett. 7 (2007) 3469–3476.
[13] P. Peng, D.J. Milliron, S.M. Hughes, J.C. Johnson, A.P. Alivisatos, R.J. Saykally, Nano Lett. 5 (2005) 1809–1813.
[14] S.B. Rawal, S. Bera, D. Lee, D.-J. Jang, W.I. Lee, Catal. Sci. Technol. 3 (2013) 1822–1830.
[15] J. Hensel, G. Wang, Y. Li, J.Z. Zhang, Nano Lett. 10 (2010) 478–483.
[16] K. Shin, S.i. Seok, S.H. Im, J.H. Park, Chem. Commun. 46 (2010) 2385–2387.
[17] C. Wang, R.L. Thompson, J. Baltrus, C. Matranga, J. Phys. Chem. Lett. 1 (2009) 48–53.
[18] S.-C. Lo, C.-F. Lin, C.-H. Wu, P.-H. Hsieh, J. Hazard. Mater. 114 (2004) 183–190.
[19] H. Liu, L. Gao, J. Am. Ceram. Soc. 88 (2005) 1020–1022.
[20] J.-C. Lee, T.G. Kim, H.-J. Choi, Y.-M. Sung, Cryst. Growth Des. 7 (2007) 2588–2593.
[21] L. Yang, S. Luo, R. Liu, Q. Cai, Y. Xiao, S. Liu, F. Su, L. Wen, J. Phys. Chem. C 114 (2010) 4783–4789.
[22] C.-S. Lim, M.-L. Chen, W.-C. Oh, Bull. Korean Chem. Soc. 32 (2011) 1657–1661.
[23] S.B. Rawal, A.K. Chakraborty, Y.J. Kim, H.J. Kim, W.I. Lee, RSC Adv. 2 (2012) 622–630.
[24] W. Ho, J.C. Yu, J. Lin, J. Yu, P. Li, Langmuir 20 (2004) 5865–5869.
[25] J. Yu, Y. Hai, M. Jaroniec, J. Colloid Interface Sci. 357 (2011) 223–228.
[26] J. Yu, J. Zhang, M. Jaroniec, Green Chem. 12 (2010) 1611–1614.
[27] F.A. Frame, F.E. Osterloh, J. Phys. Chem. C 114 (2010) 10628–10633.
[28] M.A. Holmes, T.K. Townsend, F.E. Osterloh, Chem. Commun. 48 (2012) 371–373.
[29] C. Wang, R.L. Thompson, P. Ohodnicki, J. Baltrus, C. Matranga, J. Mater. Chem. 21 (2011) 13452–13457.
[30] W. Ho, J.C. Yu, J. Mol. Catal. A: Chem. 247 (2006) 268–274.
[31] J.B. Sambur, S.C. Riha, D. Choi, B.A. Parkinson, Langmuir 26 (2010) 4839–4847.
[32] W. Lee, S.H. Kang, S.K. Min, Y.-E. Sung, S.-H. Han, Electrochem. Commun. 10 (2008) 1579–1582.
[33] Z. Pan, H. Zhang, K. Cheng, Y. Hou, J. Hua, X. Zhong, ACS Nano 6 (2012) 3982–3991.
[34] H. Choi, P.K. Santra, P.V. Kamat, ACS Nano 6 (2012) 5718–5726.
[35] N.s. Guijarro, T. Lana-Villarreal, I.n. Mora-Sero′, J. Bisquert, R. Go′mez, J. Phys. Chem. C 113 (2009) 4208–4214.
[36] A.L. Rogach, A. Kornowski, M. Gao, A. Eychmüller, H. Weller, J. Phys. Chem. B 103 (1999) 3065–3069.
[37] F. Xiao, J. Mater. Chem. 22 (2012) 7819–7830.
[38] R. Asahi, T. Morikawa, T. Ohwaki, K. Aoki, Y. Taga, Science 293 (2001) 269–271.
[39] W. Tian, W. Mi, J. Tian, J. Jia, X. Liu, Z. Zhu, J. Dai, X. Wang, Analyst 138 (2013) 1570–1580.
[40] W. Li, D. Li, Z. Chen, H. Huang, M. Sun, Y. He, X. Fu, J. Phys. Chem. C 112 (2008) 14943–14947.
[41] L. Ge, J. Liu, Appl. Catal., B: Environ. 105 (2011) 289–297.
[42] G. Zhao, L. Jiang, Y. He, J. Li, H. Dong, X. Wang, W. Hu, Adv. Mater. 23 (2011) 3959–3963.
[43] W.I. Nawawi, M.A. Nawi, J. Mol. Catal. A: Chem. 374–375 (2013) 39–45.
[44] Zuze Mu, Synthesis, Photostability and Photocatalytic Properties of Water-suspended CdSe and CdSe/CdS Quantum Dots, Houston, TX, 2005.
[45] Y.-S. Li, F.-L. Jiang, Q. Xiao, R. Li, K. Li, M.-F. Zhang, A.-Q. Zhang, S.-F. Sun, Y. Liu, Appl. Catal., B: Environ. 101 (2010) 118–129.
[46] D.-S. Kong, Langmuir 24 (2008) 5324–5331.
[47] V. Spagnol, E. Sutter, C. Debiemme-Chouvy, H. Cachet, B. Baroux, Electrochim. Acta 54 (2009) 1228–1232.
[48] M.W. Kanan, D.G. Nocera, Science 321 (2008) 1072–1075.
[49] A. Ishikawa, T. Takata, J.N. Kondo, M. Hara, H. Kobayashi, K. Domen, J. Am. Chem. Soc. 124 (2002) 13547–13553.
[50] W. Li, D. Li, S. Meng, W. Chen, X. Fu, Y. Shao, Environ. Sci. Technol. 45 (2011) 2987–2993.
[51] H. Liu, S. Cheng, M. Wu, H. Wu, J. Zhang, W. Li, C. Cao, J. Phys. Chem. A 104 (2000) 7016–7020.
[52] I. Robel, M. Kuno, P.V. Kamat, J. Am. Chem. Soc. 129 (2007) 4136–4137.
[53] A. Ye, W. Fan, Q. Zhang, W. Deng, Y. Wang, Catal. Sci. Technol. 2 (2012) 969–978.
[54] W. Li, D. Li, W. Zhang, Y. Hu, Y. He, X. Fu, J. Phys. Chem. C 114 (2010) 2154–2159.
[55] Y. Lin, D. Li, J. Hu, G. Xiao, J. Wang, W. Li, X. Fu, J. Phys. Chem. C 116 (2012) 5764–5772.
[56] R. Palominos, J. Freer, M.A. Mondaca, H.D. Mansilla, J. Photochem. Photobiol., A: Chem. 193 (2008) 139–145.
[57] C. Chen, P. Lei, H. Ji, W. Ma, J. Zhao, H. Hidaka, N. Serpone, Environ. Sci. Technol. 38 (2003) 329–337.
[58] H. Bader, V. Sturzenegger, J. Hoigné, Water Res. 22 (1988) 1109–1115.
[59] S. Meng, D. Li, M. Sun, W. Li, J. Wang, J. Chen, X. Fu, G. Xiao, Catal. Commun. 12 (2011) 972–975.